However, it is possible that the observed behavior of the state is atypical of the ensemble. To characterize the ensembles as a whole, it is necessary to gather statistics over all the states, or at least a Monte Carlo sample of them. We do this by plotting the *interface plumes*, that is, the sum of the interfaces of the states in each two-domain ensemble. For each of the ensembles plotted in fig. 11.8, we generated a Monte Carlo sample of $M = 1000$ states of size $N = 1000$, and evolved each state up to time $t = 200$. The structure of the plumes is made clearer by plotting the mean left edge $\mu_{\rm L}$, the center $\mu_{\rm C}$, and the mean right edge $\mu_{\rm R}$, defined in section 9.6.

The three quantities $\mu_{\rm L}$, $\mu_{\rm C}$ and $\mu_{\rm R}$ are plotted vs. time in fig. 11.9, for the same ensembles as in fig. 11.8. They are the three solid lines in each plot, with $\mu_{\rm L}(t) \leq \mu_{\rm C}(t) \leq \mu_{\rm R}(t)$ for all $t$. In addition to the mean quantities, $\mathrm{Left}(\theta_t)$ and $\mathrm{Right}(\theta_t)$, the respective positions of the left-most and right-most wall detected at each time, are plotted as dashed lines.

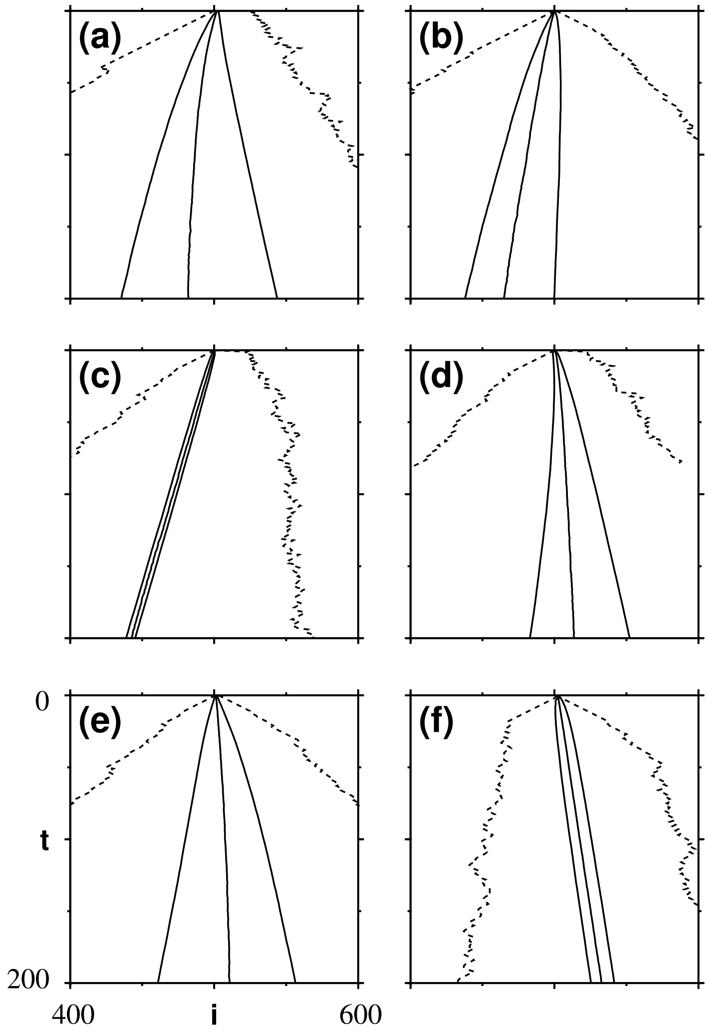


Fig. 11.9 Interface plumes for ensembles of the six types of state shown in fig. 11.8. The labels (a) — (f) denote the same ensembles as in that figure.

Figs. 11.9(a) and 11.9(e) are similar, though plume (a) drifts slowly left, while plume (e) drifts slowly right. States in both of these ensembles are of the "spreading interface" type. The plume of fig. 11.9(b) also spreads, though more slowly than plumes (a) and (e); in addition it shows a faster net drift to the left.

Fig. 11.9(d) shows a slower rate of spreading, though it is still nonzero. This indicates that the apparently localized interface shown in fig. 11.8(d) is atypical of the ensemble. While some initial conditions have interfaces that remain localized, there are others in which it spreads more in the fashion of fig. 11.8(a), 11.8(b) or 11.8(e). This suggests that the ensemble plotted in fig. 11.9(d) is composed of sub-ensembles with qualitatively different behavior. It is interesting to note that $\mu_{\mathrm{L}}(t)$ moves to the left at first, but then slowly curves back to the right. We do not at this point have an explanation for this highly unusual behavior.

Figs. 11.9(c) and 11.9(f), on the other hand, show little or no spreading at all. After an initial growth period, the distance $\mu_{\mathrm{R-L}} = \mu_{\mathrm{R}} - \mu_{\mathrm{L}}$ remains a small constant value. This correlates well with the behavior seen in figs. 11.8(c) and 11.8(f). The mean drift velocity, given by the slope of $\mu_{\mathrm{C}}$, is surprisingly constant, although as the dashed lines indicate, there is a great deal of variation in the individual trajectories. It appears that for these two ensembles, the interface does behave as a "particle", at least in an average sense.

Least-squares fits of the curves of $\mu_{\mathrm{R-L}}(t)$ vs. $t$ indicated that plumes (a), (b), and (e) are well described by a power law $\mu_{\mathrm{R-L}}(t) \propto t^{\alpha}$ with the exponents as follows: (a) $\alpha = 0.80$; (b) $\alpha = 0.67$; (e) $\alpha = 0.79$. Plumes (c) and (f) for long times ($t > 100$) showed very slow linear growth $\mu_{\mathrm{R-L}}(t) = mt + const$ with rates of $m = 0.008$ for plume (c) and $m = 0.04$ for plume (f). The curve for plume (d) was nearly a straight line, with a fit to a quadratic polynomial $\mu_{\mathrm{R-L}}(t) = a + bt + ct^2$ giving coefficients $a = 2.9$, $b = 0.29$ and $c = 2.1 \times 10^{-4}$.

As we observed in the last subsection, the evolution of walls in the plots of fig. 11.8 appears to be a diffusive process. One very rough measure of the diffusivity of wall motion is given by the growth in the standard deviation $\sigma(t)$ of the distribution of walls in the interface. This statistic neglects the fact that many walls may be present in a single interfacial region, and that those walls are constantly interacting, annihilating each other and giving birth to multiple offspring. Nevertheless it serves to give an indication of the average evolution of the ensemble. For comparison with what follows, we note that the expected form for an ideal random walk is $\sigma(t) = Dt^{1/2}$ with $D$ constant. For each of the ensembles shown in fig. 11.9, we measured $\sigma(t)$ for $0 \leq t \leq 200$ and fitted the resulting curve to both power-law and exponential functional forms. For $t \geq 10$, all six curves showed power-law growth $\sigma(t) \propto t^{\alpha}$ with the following exponents: plumes (a), (b), (d), and (e) all had $\alpha = 0.6$, plume (c) had $\alpha = 0.5$, and plume (f) had $\alpha = 0.4$.

The plume volume $\xi_{\mathcal{L}}(t)$ provides another test of whether the interface is behaving as a particle or whether it is unstable. Plots of $\xi_{\mathcal{L}}(t)$ vs. $t$ for the six ensembles of figs. 11.8 and 11.9 are shown in fig. 11.10. Since a particle is by definition localized

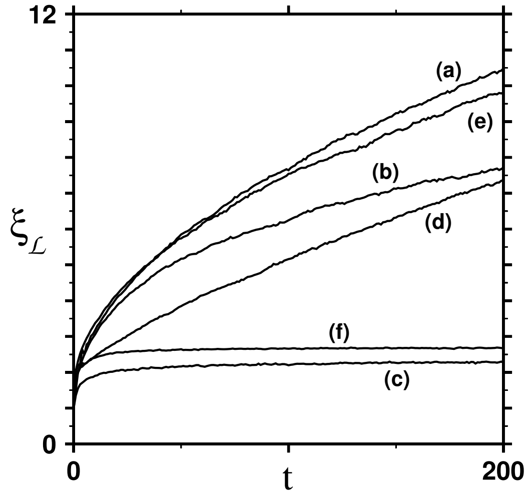


Fig. 11.10 Interface plume volumes $\xi_{\mathcal{L}}(t)$ vs. $t$. The labels (a) — (f) denote the same ensembles as in figs. 11.8 and 11.9.

in space, it necessarily must have a roughly constant—or at least bounded—number of walls. This indeed is the case for curves (c) and (f) of fig. 11.10. After an initial period of rapid growth, they flatten out so that by $t \approx 100$ they are both roughly constant. It is interesting to note, however, that the average number of walls in the two "particles" differ. The values of $\xi_{\mathcal{L}}(t)$ for the two plumes, averaged over times $100 \leq t \leq 200$, were $\overline{\xi_{\Lambda^{1,0}}} = 2.26 \pm 0.05$ for curve (c) and $\overline{\xi_{\Lambda^{1,1}}} = 2.67 \pm 0.02$ for curve (f).

In addition, the curves in fig. 11.10 appear to fall into three classes: curves (a), (e) and (b) all have similar shape, as do curves (f) and (c). The third class is exemplified by curve (d). Note that it was ensemble (d) whose plume showed interesting spreading properties (fig. 11.9(d)). Least-squares fits to exponential, power-law and polynomial functional forms indicated that curves (a), (b) and (e) showed power-law growth $\xi \propto t^{\alpha}$ with exponents of $\alpha = 0.36$ for both (a) and (e), and $\alpha = 0.30$ for (b). Curve (d) was best fit by a quadratic polynomial $\xi = a + bt + ct^2$ with $a = 2.08$, $b = 0.035$ and $c = -4.7 \times 10^{-5}$.

There is clearly room for further investigation into the behavior of domain interfaces. We have only touched on the phenomenology, without even attempting to trace the causal mechanisms responsible for the different behaviors. Nevertheless, we want to emphasize that without the simplification accomplished by identifying the domains, we would never have even gotten this far. Any analysis of domain interfaces—for example, tracing the behavior back to the CA rule table, or deriving statistical models of interface evolution—must necessarily be based on the pattern basis the domains represent.

# 12 The Attractor-Basin Portrait of ECA 18

In sections 10.5 and 10.8, we proved that the regular domain $\Lambda^0_{18}$ and the two-domain language $\Lambda^{0,0}_{18}$ are temporally invariant under ECA 18. We showed that the number of dislocations in an arbitrary initial condition is nonincreasing in time and that dislocations annihilate in pairs. We presented numerical evidence that dislocations behave as diffusing particles, annihilating when their paths cross. In this chapter and the one following it, we will continue the investigation of the qualitative dynamics of ECA 18. We will drop the subscripts on $\Lambda^0_{18}$ and $\Lambda^{0,0}_{18}$ throughout this chapter and the next, referring to these languages as $\Lambda^0$ and $\Lambda^{0,0}$.

In this chapter, we will show that $\Lambda^0$ and $\Lambda^{0,0}$ are both *stable* invariant sets: they are regular attractors. In terms of the attractors, we will define basins and separatrices. We will make use of the diffusive behavior of dislocations to discuss the evolution of typical initial conditions on typical lattices—i.e., the global evolution of ECA 18—concluding that $\Lambda^0$ and $\Lambda^{0,0}$ are the only *statistically significant* attractors. In the course of this discussion, we will construct a number of transducers for elucidating different aspects of ECA 18's behavior. Finally, we will collect all of our various results into two views of the *attractor-basin portrait* of ECA 18.*

Detailed numerical investigations of the stability of $\Lambda^0$ and $\Lambda^{0,0}$ will be presented in the following chapter, along with a quantitatively accurate stochastic model of dislocation evolution. Here, we will simply allude to the results of these investigations as needed.

## 12.1 Vicinities in ECA 18

For the vicinities $V_1(\mathcal{L})$ and $V_2(\mathcal{L})$ required by definition (2) of regular attractor (see below or section 8.2), we will take $V_1(\mathcal{L}) = V_H(\mathcal{L})$ or $V_1(\mathcal{L}) = V_r(\mathcal{L})$ as appropriate, and let $V_2(\mathcal{L})$ be a level set (or more precisely, a union of level sets) of the machine metric $\|\cdot\|_{\mathrm{M}(\Lambda^0)}$. Each of these vicinities is described in turn below for the case $\mathcal{L} = \Lambda^0$. For $\mathcal{L} = \Lambda^{0,0}$, the constructions are analogous.

In ECA 18, the "quiescent" cell is $\hat{\sigma} = 0$, so that the pattern $0^*$ is invariant. Thus the region of non-quiescent support (see section 8.1) used in the construction of $V_r$ is synonymous with the region of nonzero support, i.e., the smallest interval that contains all cells with nonzero values.

**Lemma.** $V^0 \equiv V_H(\Lambda^0)$, shown in fig. 12.1(a), and $V^0_{\mathrm{supp}} \equiv V_r(\Lambda^0)$, shown in fig. 12.1(b), are the regular Hamming vicinity and the restricted Hamming vicinity of $\Lambda^0$, respectively. The subscript $\mathrm{supp}$ denotes the perturbations' restriction to the region of nonzero support.

*The attractor-basin analysis of ECA 18 originally appeared in ref. [47].

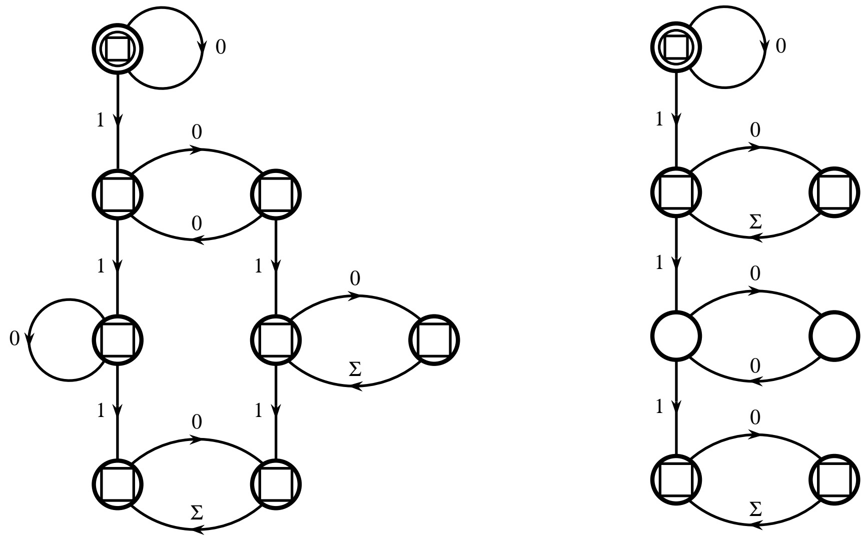

**(a)** **(b)**

Fig. 12.1 (a) The DFA for the Hamming vicinity $V^0$ of the regular domain $\Lambda^0$. (b) The DFA for the language $V^0_{\mathrm{supp}}$, formed from $\Lambda^0$ by flipping a single bit in the nonzero support of each state.

*Proof:* By explicit construction using the definitions: $V^0 = \left[\mathrm{T}_{V_H} \circ \Lambda^0\right]_{\mathrm{out}}$ and $V^0_{\mathrm{supp}} = \left[\mathrm{T}_{V_r} \circ \Lambda^0\right]_{\mathrm{out}}$. ▌

Note that $V^0_{\mathrm{supp}}$ consists of two disjoint parts: (i) states that remain in $\Lambda^0$ and (ii) states in which the perturbation generates two dislocations separated by an even number of $0$s.

As we saw in section 10.8, the number of dislocations in an arbitrary state evolving under ECA 18 is nonincreasing in time, and decreases by multiples of two as pairs of dislocations annihilate. We can use this fact to define a vicinity $V_b(\Lambda^0)$ as follows.

**Definition.** Consider the regular language $\Lambda^{0,0,0}$ consisting of all states made up of three adjacent domains $\Lambda^0$ separated by dislocations. The **subbasin vicinity**† of $\Lambda^0$ is the regular language

$$V_b(\Lambda^0) \equiv \Lambda^{0,0,0} \cup \Lambda^0. \tag{12.1}$$

Each state in $\Lambda^{0,0,0}$ has exactly two dislocations. Therefore $V_b(\Lambda^0)$ is a union of two level sets of the machine metric $\|\cdot\|_{\mathrm{M}(\Lambda^0)}$: it consists of all states $\mathrm{s}$ with $\|\mathrm{s}\|_{\mathrm{M}(\Lambda^0)} = 0$ or $2$.

Fig. 12.2(a) shows the minimal DFA for $V_b(\Lambda^0)$. Note that the machine consists of a synchronization state followed by three cyclic loops that are copies of the process graph of $\Lambda^0$ (fig. 10.14(a)). The cycles are connected by edges representing dislocations. The states in the middle copy are not accepting, consistent with the requirement that $V_b(\Lambda^0)$ consist of states with $0$ or $2$ dislocations. Comparison of

†The reason for this terminology will be made clear in a later section.

figs. 12.2(a) and 12.1(b) also shows the similarity of $\mathrm{M}\big(V_b(\Lambda^0)\big)$ and $\mathrm{M}\big(V^0_{\mathrm{supp}}\big)$: the two machines differ by a single edge label. In $\mathrm{M}\big(V_b(\Lambda^0)\big)$ this is the edge in the middle cycle labeled with $\Sigma$, denoting two parallel transitions with labels $0$ and $1$. The corresponding edge in $\mathrm{M}\big(V^0_{\mathrm{supp}}\big)$ is a single transition with label $0$. This clearly implies that $V^0_{\mathrm{supp}} \subset V_b(\Lambda^0)$.

**Lemma.** The subbasin vicinity $V_b(\Lambda^0)$ is a regular vicinity of $\Lambda^0$. Further, $V_b(\Lambda^0)$ is a trapping region.

*Proof:* As fig. 12.2(a) shows, $V_b(\Lambda^0)$ is a regular language and $\Lambda^0 \subset V_b(\Lambda^0)$; therefore $V_b(\Lambda^0)$ is a regular vicinity of $\Lambda^0$. Because dislocations annihilate in pairs, states with $2$ dislocations evolve to states with $2$ or $0$ dislocations. Equivalently, each of the languages $\mathbf{\Phi}^t(\Lambda^{0,0,0})$, $t \geq 0$, is a subset of $\Lambda^{0,0,0} \cup \Lambda^0$. Since $\Lambda^0$ is invariant, this proves that $V_b(\Lambda^0)$ is a trapping region: $\mathbf{\Phi}^t\big(V_b(\Lambda^0)\big) \subseteq V_b(\Lambda^0)$. ▌

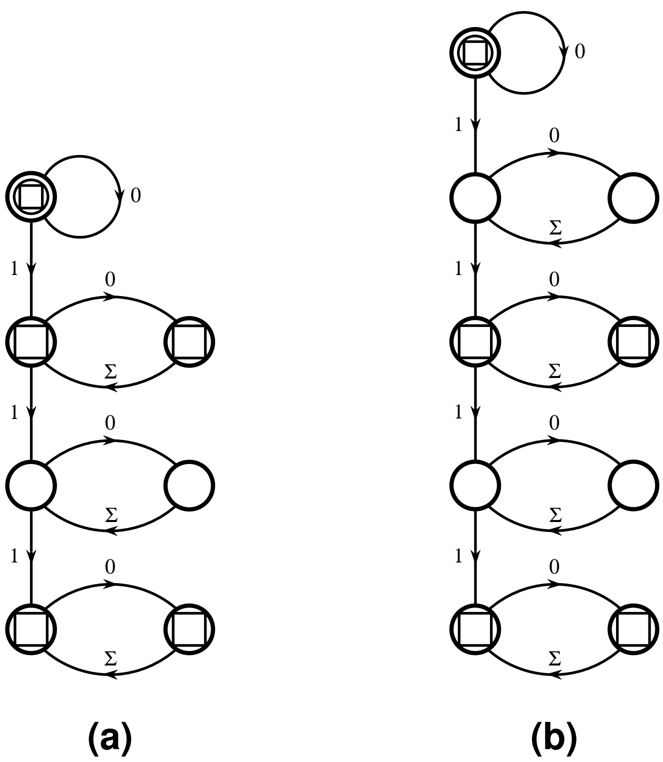


Fig. 12.2 The minimal DFA for the subbasin vicinities (a) $V_b(\Lambda^0)$ of the regular domain $\Lambda^0$ and (b) $V_b(\Lambda^{0,0})$ of the two-domain language $\Lambda^{0,0}$. After the start state devoted to synchronization, each graph consists of a number of copies of the process graph of $\Lambda^0$.

The subbasin vicinity of $\Lambda^{0,0}$ is similarly defined as

$$V_b(\Lambda^{0,0}) \equiv \Lambda^{0,0,0,0} \cap \Lambda^{0,0} \tag{12.2}$$

where $\Lambda^{0,0,0,0}$ denotes the set of states with three dislocations. Like $V_b(\Lambda^0)$, $V_b(\Lambda^{0,0})$ is a union of level sets of the machine metric, this time with $\|\mathrm{s}\|_{\mathrm{M}(\Lambda^0)} = 1$ or $3$. In addition, the pattern $0^*$ is included in $V_b(\Lambda^{0,0})$, since that pattern is in $\Lambda^{0,0}$. $V_b(\Lambda^{0,0})$ is a regular vicinity of $\Lambda^{0,0}$ and is a trapping region. Fig. 12.2(b) shows the minimal DFA $\mathrm{M}(V_b(\Lambda^{0,0}))$. As expected, $\mathrm{M}(V_b(\Lambda^{0,0}))$ consists of four copies of $\mathrm{M}(\Lambda^0)$ separated by dislocations.

## 12.2 Attractors in ECA 18

In conjunction with numerical investigations, the definitions and propositions formulated so far allow us to analyze in some detail the state space structure of ECA 18. Our goal is to establish that $\Lambda^0$ and $\Lambda^{0,0}$ are fixed-point regular attractors. In doing this we will make use of definition (2) of fixed-point regular attractor, repeated for convenience below. A previous discussion[47] of attractors in ECA 18 was flawed because it used the over-restrictive definition (1) in conjunction with the Hamming vicinity. It later turned out that the Hamming vicinity is not a trapping region, and so violates condition (i) of that definition. This section therefore constitutes a correction of that earlier version.

The argument breaks up into three cases depending on the CA lattice size and the class of initial conditions: (i) finite periodic lattices; (ii) infinite lattices with finite initial conditions; and (iii) infinite lattices with infinite initial conditions. After analyzing the cases via several observations, a proposition and a conjecture, we summarize the remaining steps for a direct proof.

Before proceeding, we repeat the definition of fixed-point regular attractor from chapter 8:

**Definition (2).** An invariant language $A$ is a **fixed-point regular attractor** if it is a regular language and there exist regular vicinities $V_1(A)$ and $V_2(A)$ such that

i. $V_1(A) \subseteq V_2(A)$;
ii. $V_2(A)$ is a trapping region: $\mathbf{\Phi}(V_2) \subseteq V_2$; and
iii. All states in $V_1(A)$, except possibly for a set $R$ such that $S(R|V_1) = 0$, eventually collapse down onto $A$: thus for almost all $\mathrm{s} \in V_1$, there exists a $t \geq 0$ such that $\Phi^t(\mathrm{s}) \in A$.

$S(R|V_1)$, defined in section 4.5, is the relative size of $R$ with respect to $V_1$.

**Observation.** For finite periodic lattices with an even number of sites $N$, $\Lambda^0$ is a fixed-point regular attractor.

*Discussion:* A previous proposition (see section 10.5) established that $\Lambda^0$ is time-invariant. We take as the regular vicinity $V_1(\Lambda^0)$ the unrestricted Hamming vicinity $V^0$, and further take $V_2(\Lambda^0) = V_b(\Lambda^0)$. The periodic boundary conditions ensure that on all lattices of even $N$, the number of dislocations is even; thus all states in $V^0$ have either $d = 0$ or $2$ dislocations: $V^0 \subset V_b(\Lambda^0)$. We have already shown that $V_b(\Lambda^0)$ is a trapping region. Thus conditions (i) and (ii) of the definition are satisfied. To show attraction, it would be sufficient to show that the fraction of states in the nonattracted set goes to zero with increasing lattice size. Numerical simulations, to be discussed in chapter 13, indicate that the upper bound on the fraction of nonattracted states obeys a power law $N^{-\alpha}$ with $\alpha \approx \frac{1}{2}$. This worst-case fraction is already below 3% on lattices with as few as 400 cells. This indicates that the size of the nonattracted set relative to $V^0$ vanishes, and so $\Lambda^0$ is an attractor.

**Observation.** For finite periodic lattices with $N$ odd, $\Lambda^{0,0}$ is a fixed-point regular attractor.

*Discussion:* The discussion is quite similar to the case for $N$ even. $\Lambda^{0,0}$ has been proven to be time-invariant. We use the unrestricted regular Hamming vicinity $V^{0,0} \equiv V_H(\Lambda^{0,0})$ for $V_1(\Lambda^{0,0})$, and the subbasin vicinity $V_b(\Lambda^{0,0})$ for $V_2(\Lambda^{0,0})$. The periodicity of the lattice ensures that $V^{0,0}$ consists, aside from the single pattern $0^*$, of states with $d = 1$ or $3$ dislocations, so that $V^{0,0} \subset V_b(\Lambda^{0,0})$. Like $V_b(\Lambda^0)$, $V_b(\Lambda^{0,0})$ is a trapping region. As in the case of $\Lambda^0$, the numerical evidence shows rapid decay of the size of the nonattracted set with increasing lattice size. Thus for periodic lattices with odd size $N$, almost all states in $V^{0,0}$ eventually fall into $\Lambda^{0,0}$, and so $\Lambda^{0,0}$ is an attractor.

Note that the behavior on finite lattices depends on whether the lattice is even or odd. For even $N$, the periodic boundary conditions require that there be an even number of dislocations in the state at all times. Since $\Lambda^{0,0}$, apart from the single state $0^*$, has a single dislocation, it will never be present on an even–sized lattice. Similarly, $\Lambda^0$ (again, apart from $0^*$) will never exist on a lattice with $N$ odd. Thus, one or the other may be present, but never both together.

By taking advantage of the domain isomorphism discussed in the next section, we can apply the well-understood algebraic analysis[65] of ECA 90 to ECA 18 to learn more about the attractors. The principal result of concern to us here is that on periodic lattices of size $N = 2^k$, all initial conditions evolve under ECA 90 to the null state $0^*$.[76] For $N \neq 2^k$, this is not the case. As we will see, the implication of this for ECA 18 is that for states with $d$ dislocations evolving on lattices of size $N = 2^k - d$, a relatively large number of states will fall directly into $0^*$ before any dislocations have annihilated. For example, for $N = 2^k$ all states in $\Lambda^0$ $(d = 0)$ eventually evolve to the single pattern $0^*$, and for $N = 2^k - 1$ all states in $\Lambda^{0,0}$ $(d = 1)$ evolve to $0^*$. Thus $0^*$ is the attracting invariant set for these lattices, and the regular attractors $\Lambda^0$ and $\Lambda^{0,0}$ are "degenerate" in the sense that only the pattern $0^*$ is actually present. Similarly, for $N = 2^k - 2$ a significant number of the states in $V^0$ that have $d = 2$ will fall directly into $0^*$, and for $N = 2^k - 3$ many of the states in $V^{0,0}$ with $d = 3$ evolve to $0^*$. However, this "leakage" into $0^*$ is typically a zero-sized effect, as the following Observation indicates.

**Observation.** Let $(\Lambda, V)$ denote the attractor and its Hamming vicinity on a finite periodic lattice of any size. That is, $(\Lambda, V) = (\Lambda^0, V^0)$ for $N$ even, and $(\Lambda, V) = (\Lambda^{0,0}, V^{0,0})$ for $N$ odd. Further, let $\mathcal{B}(0^*)$ denote the set of all states that map to $0^*$, i.e., the basin of $0^*$. Then on all but a sparse set of lattices,* $S(\mathcal{B}(0^*) \cap V|V) = 0$ and $S(\mathcal{B}(0^*) \cap \Lambda|\Lambda) = 0$.

*Discussion:* First we show that the set of lattices discussed above, for which $0^*$ is known to be an important attracting invariant set, is sparse. The set of these lattice sizes is $R_d = \{N : N = 2^k - d,\ d \in \{0, 1, 2, 3\} \text{ and } k \in \mathbb{Z}^+\}$. The number $I_{R_d}(n)$ of lattice sizes $N$ in $R_d$ such that $N \leq n$ grows as $I_{R_d}(n) = 4 \times \lfloor \log_2(n) \rfloor - \text{const.}$ for large $n$, where $\lfloor x \rfloor$ is the integer part of $x$. In the limit of large $n$, we have

$$\lim_{n \to \infty} \frac{I_{R_d}(n)}{n} = \lim_{n \to \infty} \frac{4 \log_2(n)}{n} = 0 \tag{12.3}$$

and so $R_d$ is sparse. We next investigate numerically the behavior on the remaining lattices. Simulations on lattices not in the above sparse set have shown that as a function of increasing $N$, the upper bound on the fraction of states in the attractor $\Lambda$ that map to $0^*$ decays with a power law. The same is true of the vicinity $V$. This indicates that $S(\mathcal{B}(0^*) \cap \Lambda|\Lambda) = 0$ and $S(\mathcal{B}(0^*) \cap V|V) = 0$ on all but the sparse set $R_d$ of lattices.

To analyze the behavior of ECA 18 on an infinite lattice, we must extend the notion of regular language to include words of infinite length. This extension has been considered elsewhere[80] and will not be repeated in detail here. For our purposes, it suffices to consider such an "infinitary regular language" as the set of all infinite words that can be generated by some finite automaton. This puts a restriction on the structure of the machine, in that there must be a loop containing accept states in the asymptotic part of its graph. Below, we will not differentiate between regular languages (sets of finite words) and infinitary regular languages (sets of infinite words), using the same symbol—e.g., $\Lambda^0$—for both.

On infinite lattices $\Lambda^0$ and $\Lambda^{0,0}$ coexist. To keep the attractors distinct, it is necessary to subtract from each language those states that evolve into $0^*$. To this end we define the languages

$$\begin{aligned} \tilde{\Lambda}^0 &\equiv \Lambda^0 - \mathcal{B}(0^*) \\ \tilde{\Lambda}^{0,0} &\equiv \Lambda^{0,0} - \mathcal{B}(0^*) \end{aligned} \tag{12.4}$$

where, as above, $\mathcal{B}(0^*)$ is the basin of $0^*$, and the set-theoretic difference $P - Q$ denotes the set of states in $P$ that are not in $Q$. Note that $\tilde{\Lambda}^0$ and $\tilde{\Lambda}^{0,0}$ are disjoint and time-invariant.

**Proposition.** On an infinite lattice with finite initial conditions $\mathrm{s}_0 \in 0^\omega(0+1)^*0^\omega$, $\tilde{\Lambda}^0$ and $\tilde{\Lambda}^{0,0}$ are fixed point regular attractors.

*Proof:* In the case of finite initial conditions, $0^*$ is a Gardern-of-Eden state, so $\mathcal{B}(0^*) = 0^*$. $\mathrm{M}\left(\tilde{\Lambda}^0\right)$ and $\mathrm{M}\left(\tilde{\Lambda}^{0,0}\right)$ are easily constructed from $\mathrm{M}(\Lambda^0)$ and $\mathrm{M}(\Lambda^{0,0})$, respectively shown in figs. 10.14(b) and 10.27, by making the start states nonaccepting.

*See section 2.1 for the definition of sparse set.

$\tilde{\Lambda}^0$ and $\tilde{\Lambda}^{0,0}$ are disjoint, time-invariant *regular* languages. For $V_1(\Lambda^0)$ and $V_1(\Lambda^{0,0})$ we use the restricted Hamming vicinities $\tilde{V}^0_{\mathrm{supp}} \equiv V_r(\Lambda^0) - \mathcal{B}(0^*)$ and $\tilde{V}^{0,0}_{\mathrm{supp}} \equiv V_r(\Lambda^{0,0}) - \mathcal{B}(0^*)$. For $V_2(\Lambda^0)$ and $V_2(\Lambda^{0,0})$ we use $\tilde{V}_b(\Lambda^0) \equiv V_b(\Lambda^0) - \mathcal{B}(0^*)$ and $\tilde{V}_b(\Lambda^{0,0}) \equiv V_b(\Lambda^{0,0}) - \mathcal{B}(0^*)$. As for the finite-lattice cases, $\tilde{V}^0_{\mathrm{supp}} \subset \tilde{V}_b(\Lambda^0)$ and $\tilde{V}^{0,0}_{\mathrm{supp}} \subset \tilde{V}_b(\Lambda^{0,0})$, and $\tilde{V}_b(\Lambda^0)$ and $\tilde{V}_b(\Lambda^{0,0})$ are trapping regions. To prove attraction, we quote the following results of [63]: (i) all states, apart from $0^*$, in which the initial number $n_d$ of dislocations is even, fall into $\tilde{\Lambda}^0$; and (ii) if $n_d$ is odd, then the state will fall into $\tilde{\Lambda}^{0,0}$. If we denote the set of finite initial conditions by $F$, this means in particular that all states in $\tilde{V}^0_{\mathrm{supp}} \cap F$ fall into $\tilde{\Lambda}^0$. More formally,

$$\forall\, \mathrm{s} \in \tilde{V}^0_{\mathrm{supp}} \cap F, \exists\, t < \infty \text{ such that } \Phi^t \mathrm{s} \in \tilde{\Lambda}^0. \tag{12.5}$$

Similarly, all states in $\tilde{V}^{0,0}_{\mathrm{supp}} \cap F$ fall into $\tilde{\Lambda}^{0,0}$. ▮

**Conjecture.** On an infinite lattice with infinite initial conditions, $\Lambda_\infty \equiv \Lambda^0 \cup \Lambda^{0,0}$ is a fixed point regular attractor. Specifically,

$$\Lambda_\infty = \tilde{\Lambda}^0 \cup \tilde{\Lambda}^{0,0} \cup [\mathcal{B}(0^*) \cap \Lambda_\infty] \tag{12.6}$$

with $\tilde{\Lambda}^0$ and $\tilde{\Lambda}^{0,0}$, as defined above, are disjoint, possibly non-regular, attracting invariant sets, and $S(\mathcal{B}(0^*) \cap \Lambda_\infty | \Lambda_\infty) = 0$.

*Discussion:* In the case of infinite initial conditions, $\mathcal{B}(0^*)$ is more than just $0^*$; it may or may not even be regular. If $\mathcal{B}(0^*)$ is non-regular, then $\tilde{\Lambda}^0$ and $\tilde{\Lambda}^{0,0}$ can be non-regular as well. Nevertheless, they may still be attracting. The language $\Lambda_\infty$ is clearly regular and time-invariant, since it is the union of two invariant regular languages. $\mathrm{M}(\Lambda_\infty)$ is readily formed from $\mathrm{M}(\Lambda^{0,0})$ (see fig. 10.27) by making all machine states accepting. We take $V_1 = V_\infty \equiv V^0 \cup V^{0,0}$ and $V_2 = V_b(\Lambda^0) \cup V_b(\Lambda^{0,0})$. Clearly, we have $V_1 \subset V_2$. $V_2$ consists of all states with $0,\ 1,\ 2,$ or $3$ dislocations, and is a trapping region. To argue for attraction, we partition $V_\infty$ into the disjoint, possibly non-regular, sets $\tilde{V}^0 \equiv V^0 - \mathcal{B}(0^*)$, $\tilde{V}^{0,0} \equiv V^{0,0} - \mathcal{B}(0^*)$, and $\mathcal{B}(0^*)$. The preceding Observations indicate that almost all states in $\tilde{V}^0$ and $\tilde{V}^{0,0}$ eventually fall into $\tilde{\Lambda}^0$ and $\tilde{\Lambda}^{0,0}$, respectively. By definition, all states in $\mathcal{B}(0^*)$ evolve to the invariant state $0^*$. We consider only $\tilde{\Lambda}^0$ in detail, since the discussion for $\tilde{\Lambda}^{0,0}$ is quite similar. The third Observation above indicates that in the limit of infinite $N$, $\mathcal{B}(0^*)$ has zero size relative to $\Lambda^0$ and $V^0$. Equivalently, $S\left(\tilde{\Lambda}^0 | \Lambda^0\right) = \mathcal{O}(1)$ and $S\left(\tilde{V}^0 | V^0\right) = \mathcal{O}(1)$. So, we can concentrate on $V^0$ and $\Lambda^0$ since they differ from $\tilde{V}^0$ and $\tilde{\Lambda}^0$ by a set of zero size. To show that almost all states in $\tilde{V}^0$ eventually fall into $\tilde{\Lambda}^0$, it is sufficient to show that almost all states in $V^0$ fall into $\Lambda^0$.

The set $V^0$ breaks up into three disjoint subsets:

i. $\left\{\mathrm{s} : \Phi^t \mathrm{s} \in \Lambda^0 \text{ for some } t < \infty\right\}$. This is by far the largest set. Indeed, half of the states in $V^0$ have $0$ dislocations, and hence are already in $\Lambda^0$ at $t = 0$.
ii. $\left\{\mathrm{s} : \Phi^t \mathrm{s} \underset{t\to\infty}{\longrightarrow} \text{temporally periodic state in } V_b(\Lambda^0) - \Lambda^0\right\}$. The temporal periodicity implies that s is spatially periodic. This is because of the expanding nature of

ECA 18: local site information is transmitted along the lattice in both directions at the speed of light. If the state as a whole is to be temporally periodic, it must be due to an underlying spatial periodicity. Since a spatially periodic state of period $p$ evolving on an infinite lattice is equivalent to a primitive period of that state evolving on a finite periodic lattice of $p$ cells, this set falls into the case of the first Observation above, which indicates that it is of vanishing size.

iii. $\left\{ \mathrm{s} : \Phi^t \mathrm{s} \underset{t\to\infty}{\rightarrow} \text{temporally aperiodic state in } V_b\left(\Lambda^0\right) - \Lambda^0 \right\}$. This is the "quasiperiodic" case in which the two dislocations either diverge forever from each other or march along the lattice roughly in parallel, their velocities having the same sign. It is not yet certain whether such states even exist. At the very least, if they do, they are extremely rare, and we ignore them.

The net result is that in the limit $t \to \infty$ at most a set of vanishing size remains outside of $\Lambda^0$. Almost all states in $V^0$ eventually fall into $\Lambda^0$ and so $\tilde{\Lambda}^0$ is attracting. As we said, similar arguments show that $\tilde{\Lambda}^{0,0}$ is attracting and that $S\left(\mathcal{B}(0^*) \cap \Lambda^{0,0} | \Lambda^{0,0}\right) = 0$. Putting the two cases together immediately gives that $\Lambda_\infty$ is a regular attractor, and that $S(\mathcal{B}(0^*) \cap \Lambda_\infty | \Lambda_\infty) = 0$.

We expect to be able to use the language-theoretic apparatus we have set up to rigorously demonstrate the attracting nature of $\Lambda^0$ and $\Lambda^{0,0}$. This will be left for presentation elsewhere. The strategy to be used is as follows. We define $\widehat{V}^0 = V^0_{\mathrm{supp}} - \Lambda^0$, and evolve this language forward in time using the FME algorithm, at each time step excising those states which have fallen into $\Lambda^0$. In this way, we examine the timeseries of languages

$$\widehat{V}^0_t = \mathbf{\Phi}\left(\widehat{V}^0_{t-1}\right) - \Lambda^0, \text{ with } \widehat{V}^0_0 = V^0_{\mathrm{supp}} - \Lambda^0 \tag{12.7}$$

This is the set of vicinity patterns that have not fallen onto the attractor. Our goal is to find sufficient regularity in the time series to make it possible to bound the decay in the size of $\widehat{V}^0_t$ as $t \to \infty$. If the asymptotic size is zero, then attraction is proved. The conjecture is that there is a monotonic decrease in the upper bound on the size of the nonattracted set and that this decay rate can be estimated by a functional renormalization equation determined by the CA rule acting on the defined ensemble. The spatial rescaling should reveal with increased lattice size a "fractal" structure. The critical exponent associated with the self-similarity will describe that set and determine the size decay rate. All we require is monotonic decrease, a fairly lenient property compared to those used in the existing algebraic and combinatorial analyses.

The arguments in this section employed both proof and numerical observation. The remaining steps necessary to turn them into rigorous propositions can be laid out in detail:

i. Prove that the sets of nonattracted states in $V^0$ and $V^{0,0}$ have zero size relative to $\Lambda^0$ and $\Lambda^{0,0}$ for typical $N$. The algebraic analysis might help carry this out by calculating the number of nonattracted periodic orbits in the vicinity, providing bounds on the number-theoretic fluctuations over finite lattices.

ii. Prove that $\mathcal{B}(0^*)$ has zero size relative to $\Lambda^0$ and $\Lambda^{0,0}$ on all but a sparse set of lattices.
iii. Prove that the set of aperiodic nonattracted states in $V_\infty$ on an infinite lattice with infinite initial conditions has zero size relative to $\Lambda_\infty$.

In this way the formalism we have introduced has reduced the overall problem to these three cases. Each requires that a given set have vanishing size. The numerical investigations indicate that the sizes of the above three sets rapidly decay with increasing lattice size.

A simple summary follows from accepting the numerical evidence: the regular attracting domain $\Lambda^0$ organizes the state space. Disregarding for the moment $\mathcal{B}(0^*)$, we can consider $\Lambda^{0,0}$ as the lowest "energy" fluctuation above the vacuum state $\Lambda^0$. Like analogous situations with topological solitons the dislocation in $\Lambda^{0,0}$ is stabilized by the global topology of either finite odd-size or infinite lattices. And so $\Lambda^{0,0}$ is an attractor, although not a domain.

## 12.3 Basins and Separatrix Structure

The basin of $\Lambda^0$ consists of those configurations, aside from $\Lambda^0$ itself, that have an even number of dislocations, but do not converge to temporally periodic or quasiperiodic states with dislocations. That is,

$$\mathcal{B}(\Lambda^0) = \Lambda^0 \bigcup \left\{ \mathrm{s} \in \mathcal{A}^N : \|\mathrm{s}\|_{\mathrm{M}(\Lambda^0)} = 2n, n = 1, 2, \ldots, \text{ and } \lim_{t\to\infty} \left\|\Phi^t(\mathrm{s})\right\|_{\mathrm{M}(\Lambda^0)} = 0 \right\} \tag{12.8}$$

Similarly, for $\Lambda^{0,0}$ we have

$$\mathcal{B}(\Lambda^{0,0}) = \Lambda^{0,0} \bigcup \left\{ \mathrm{s} \in \mathcal{A}^N : \|\mathrm{s}\|_{\mathrm{M}(\Lambda^0)} = 2n+1, n = 1, 2, \ldots, \lim_{t\to\infty} \left\|\Phi^t(\mathrm{s})\right\|_{\mathrm{M}(\Lambda^0)} = 1 \right\} \tag{12.9}$$

As we will see, $\Lambda^0$ and $\Lambda^{0,0}$ are the only important attractors. Since we are concerned with typical behavior, we collect into the global separatrix $\mathcal{S}$ all spatial states that do not evolve into $\Lambda^0$ or $\Lambda^{0,0}$. For example, we include in $\mathcal{S}$ any other attractors, if they exist, since the numerical results indicate that they have vanishing size relative to $\Lambda^0$ and $\Lambda^{0,0}$. We can formally write this in set theoretic notation as

$$\mathcal{S} = \mathcal{A}^N - \mathcal{B}(\Lambda^0) - \mathcal{B}(\Lambda^{0,0}) \tag{12.10}$$

The global separatrix is also the set of states for which the number of dislocations remains greater than 1 forever. As we noted above, one set for which this is true is the set of temporally periodic states with more than one dislocation. Examples of this are readily obtained by looking at periodic lattices with only a few cells. For instance, the spatial configuration $(1000010000100010)^*$, with two dislocations in the basic pattern, when iterated on periodic lattices with $N = 16m,\ m \geq 1$, or $N$ infinite, has temporal period $p = 14$. As we will see in chapter 13, the set of these nonattracted orbits has zero size. For an infinite lattice there are also quasiperiodic orbits, in which, for example, two dislocations (i) travel away from each other forever or (ii) translate in parallel with a roughly constant or periodic separating distance.

We identify three disjoint subsets of the separatrix $\mathcal{S} = \mathcal{S}_{\text{even}} \bigcup \mathcal{S}_{\text{odd}} \bigcup \mathcal{S}_{\infty}$. $\mathcal{S}_{\text{even}}$ contains those periodic orbits, and their preimages, with an even number of dislocations greater than one; $\mathcal{S}_{\text{odd}}$ has an odd number greater than one. $\mathcal{S}_{\infty}$ contains all the aperiodic, quasiperiodic orbits and their preimages.

The foregoing analysis specifies the attractor-basin portrait. The remaining problems include identifying the complexity class of the basins and separatrices and giving their finite descriptions, if such exist. We leave these to the future.

## 12.4 Global Structure of ECA 18

Having defined some of the fundamental structural objects in language space, we can now put them together with a discussion of certain behavioral properties determined by the global organization of the state space, to come up with a fairly complete picture of the overall behavior of ECA 18. The main question is the following: What usually happens to a typical initial configuration as it evolves in time? By "typical", we mean in particular "almost all configurations on almost all lattices". Atypical behavior is best treated as a refinement of the overall picture we present here, to be addressed only *after* the typical behavior is understood. In discussing the attractors, therefore, we will use $\Lambda^0$ and $\Lambda^{0,0}$ for both finite and infinite lattices, with the understanding that we are disregarding the sparse set of finite lattices for which a significant fraction of states evolve to $0^*$, and on the remaining lattices, the nonattracted sets of zero size in the vicinity of each attractor. For the infinite case, this last includes $\mathcal{B}(0^*)$ as well.

As a first step, we note again that we can treat any initial state s as a concatenation of domains of various lengths, separated by dislocations. Then a large part of the question is to decide what happens to these dislocations as the state evolves in time. We quote again the following lemma from chapter 10:

**Lemma**.[65] The number of dislocations in an arbitrary CA state evolving under ECA 18 decreases or remains constant in time. Furthermore, for all states except those that evolve immediately to the null state, dislocations always annihilate in pairs.

The domain walls appear to execute a random walk on the lattice, as we saw in section 10.8. Thus we can model the global behavior of ECA 18 with a stochastic model of diffusing, annihilating dislocations evolving against a background consisting of subsequences in the chaotic domain $\Lambda^0$.

The consequence of diffusing dislocations for ECA 18, given sufficiently large and typical $N$, is that almost every initial configuration in $\mathcal{A}^N$ eventually goes to a regular attractor: either to $\Lambda^0$ if $N$ is even, or to $\Lambda^{0,0}$ if $N$ is odd. Requiring that $N$ be typical excludes the sparse set of lattices for which $0^*$ is an important attracting invariant set. There is an even number of dislocations in any initial condition on an even lattice. And so with probability 1, the state will eventually evolve into $\Lambda^0$ on an even lattice. If $N$ is odd, the number of dislocations is always odd due to pairwise annihilation. And so, almost all initial conditions on an odd lattice eventually fall into $\Lambda^{0,0}$. The same argument holds for the case when $N$ is infinite, but the initial condition has a finite number of dislocations. On infinite lattices with infinite initial conditions the dislocation density asymptotically falls to zero, and hence any finite subsequence in the state falls into $\Lambda^0$ with probability 1. Under the assumption of diffusive motion, then, $\Lambda^0$ and $\Lambda^{0,0}$ are the only two statistically significant attractors.

The central conclusion to be drawn from this discussion is that dislocations annihilate, leading eventually to simpler, *not* more complex, spatial patterns. This conclusion is in direct opposition to the global analysis discussed in section 2.5. Recall from that section that the iterates $\Omega_t$ of the extended state space $\Omega_0 = \mathcal{A}^*$ give the set of all possible states of the system at each time $t$. For ECA 18, the size of the global machine, denoted by $V_t = \|\mathrm{M}(\Omega_t)\|$, grows extremely rapidly: $V_1 = 5$, $V_2 = 47$, $V_3 = 143$, and $V_4$ was estimated to be greater than $2 \times 10^4$.[55] The global machine blows up due to the complexity of the motion of all possible dislocations implicit in the initial ensemble of all possible configurations. There are many routes of evolution onto the attractors, and thus very large machines will persist for arbitrarily long times. The exact topological analysis necessarily includes these, but is unfortunately also dominated by them.† Consequently, these machines obscure important features such as the *typicalness* of the patterns observed and the simple decomposition into domains and walls. The simple, observed fact is that the number of dislocations is almost always decreasing. This means that ultimately the spatial patterns, for all initial conditions but a vanishingly small set, asymptotically becomes quite simple.

There is undoubtedly a deep connection between the apparent diffusivity of the dislocations and the structure of the attractors $\Lambda^0$ and $\Lambda^{0,0}$. The exact nature of that connection, and the particular mechanism by which the randomness of the initial ensemble is transformed into space-time random walks, remain open questions. Nevertheless, the greater part of the behavior of ECA 18 is described by the picture of computationally simple domains bounded by dislocations that wander about at random, annihilating as they collide.

## 12.5 Transducers for Global Structure Detection

Given this identification of the gross behavior of ECA 18, we can organize our discussion around the observed domains and the dislocations between them. In

†We note that the direct probabilistic generalization of the FME algorithm also obscures this structure, since it carries along the full topology in the support and also is sensitive to all variations in the initial configuration distribution.[71]

doing so, we will find use for three different transducers, all based on the domain language $\Lambda^0$: the machine metric $\|\mathrm{s}\|_{\mathrm{M}(\Lambda^0)}$ that counts the number of dislocations in a spatial state $\mathrm{s}$, an intercalation operator $\mathrm{T}_{\mathtt{intercalate}}(\Lambda^0)$, and a domain isomorphism $\mathrm{T}_{\mathtt{decimate}}(\Lambda^0)$. The machine metric was introduced in section 4.6 above in a more general context. The remaining two transducers are defined here.

The site-intercalation transducer $\mathrm{T}_{\mathtt{intercalate}}(\Lambda^0)$, shown in fig. 12.3, is a machine for removing dislocations by adding extra sites to the lattice. Within a domain it is the identity on all transitions, i.e. $0|0$ and $1|1$, but when a wall is detected we put $1|01$. The result is a many-to-one mapping from arbitrary patterns to patterns in $\Lambda^0$. By inserting the additional $0$, the wall is effectively removed. The mapping $f_{\mathrm{T}_{\mathtt{intercalate}}(\Lambda^0)} : \mathcal{A}^* \rightarrow \Lambda^0$ is equivalent to the global linearization operator $G(\mathrm{s})$ of ref. [63]. Since the evolution of $\Lambda^0$ is identical in ECA 18 and ECA 90, this operator linearizes ECA 18 in the sense that the rule becomes equivalent to the linear, superposition- preserving dynamics of ECA 90.

This type of global linearization applies only to patterns consisting of domains of the same type, i.e. the same regular language. For CA with more than one domain type $\{\Lambda^i\}$, such global linearization does not exist over the entire state space. Rather it appears only on subspaces composed of configurations with domains of the same type.

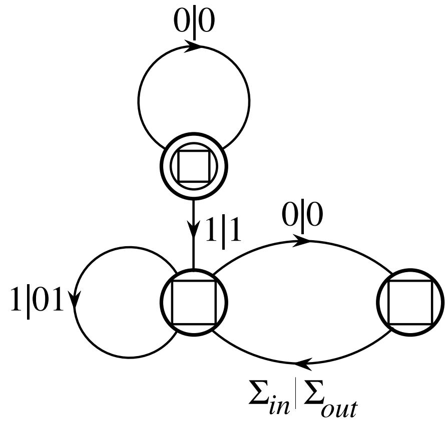


Fig. 12.3 Transducer $\mathrm{T}_{\mathtt{intercalate}}(\Lambda^0)$ for inserting new sites at dislocations. The result of such an operation is a global linearization of ECA 18.[63] Note that when a dislocation is detected two symbols, rather than one, are emitted. The transducer takes length $N$ strings to length $(N+d)$ strings, where $d$ is the number of dislocations in the input string.

The domain isomorphism transducer $\mathrm{T}_{\mathtt{decimate}}(\Lambda^0)$ (fig. 12.4(a)) demonstrates in a transparent manner that ECA 18 acting on $\Lambda^0$ is equivalent under decimation to ECA 90 acting on $\mathcal{A}^*$. Its effect is to drop the (predictable) 0 transition from the input pattern. This can also be considered an encoding and is, in fact, a compression of the input pattern. The corresponding function $f_{\mathrm{T}_{\mathtt{decimate}}(\Lambda^0)} : \Lambda^0 \rightarrow \mathcal{A}^*$ maps the domain patterns of ECA 18 onto the full extended state space. It is important to point out that in general decimation of space-time patterns requires both a space-like machine to decimate spatial configurations and a time-like machine to decimate in time. The proper framework for this requires introducing space-time machines which would take us too far afield. In this particular example the issue can be effectively skirted because the space, time, and space-time machines are identical.

One must also look at the effect of $f_{\mathrm{T}_{\mathrm{decimate}(\Lambda^0)}}$ on the rule table. From this we find the machine commutation relation

$$\mathrm{T}_{90} \circ \mathrm{T}_{\mathrm{decimate}(\Lambda^0)} = \mathrm{T}_{\mathrm{decimate}(\Lambda^0)} \circ \mathrm{T}_{18}^2 \tag{12.11}$$

In terms of languages, direct comparison of the space-time patterns shows that the action of ECA 18 on neighborhoods of size five after two time steps is identical to ECA 90 acting on neighborhood of size three after one time step, when one drops intervening zeros:

$$\begin{array}{ccccc}
\cdots\ 0\ \ \sigma_t^{i-2}\ \ 0\ \ \sigma_t^{i}\ \ 0\ \ \sigma_t^{i+2}\ \ 0\ \ \cdots & \xrightarrow[\mathrm{T}_{\mathrm{decimate}}]{} & & & \\
& & \cdots\ \sigma_t^{i-2}\ \ \sigma_t^{i}\ \ \sigma_t^{i+2}\ \cdots & & \\
\cdots\ \sigma_{t+1}^{i-3}\ \ 0\ \ \sigma_{t+1}^{i-1}\ \ 0\ \ \sigma_{t+1}^{i+1}\ \ 0\ \ \sigma_{t+1}^{i+3}\ \cdots & & & & \\
& & \cdots\ \sigma_{t+2}^{i-2}\ \ \sigma_{t+2}^{i}\ \ \sigma_{t+2}^{i+2}\ \cdots & & \\
\cdots\ 0\ \ \sigma_{t+2}^{i-2}\ \ 0\ \ \sigma_{t+2}^{i}\ \ 0\ \ \sigma_{t+2}^{i+2}\ \ 0\ \ \cdots & \xrightarrow[\mathrm{T}_{\mathrm{decimate}}]{} & & &
\end{array} \tag{12.12}$$

where $\sigma \in \mathcal{A}$. In other words, we have the language commutation relation

$$\Phi_{90} \circ f_{\mathrm{T}_{\mathrm{decimate}(\Lambda^0)}}(\Lambda^0) = f_{\mathrm{T}_{\mathrm{decimate}(\Lambda^0)}} \circ \Phi_{18}^2(\Lambda^0) \tag{12.13}$$

Thus, not only is there an equivalence on patterns, but also on the action of the rules. The transducer implements this directly, being the projection operator for the associated commuting diagram

$$\begin{array}{ccc}
\Lambda^0 & \xrightarrow{\Phi_{18}^2} & \Lambda^0 \\
f_{\mathrm{T}_{\mathrm{decimate}(\Lambda^0)}} \downarrow & & \downarrow f_{\mathrm{T}_{\mathrm{decimate}(\Lambda^0)}} \\
\mathcal{A}^* & \xrightarrow[\Phi_{90}]{} & \mathcal{A}^*
\end{array} \tag{12.14}$$

If we minimize $\mathrm{T}_{\mathrm{decimate}}(\Lambda^0)$ with respect to the output alphabet, then we obtain $\mathcal{A}^*$, which is invariant under ECA 90. One consequence is that ECA 18 is linear on the domain in the sense that $\mathbf{\Phi}(\Lambda^0)$ obeys a linear superposition in space-time (see also ref. [63]).

The domain isomorphism also provides a way of investigating the stability of the nested sub-domains $\Lambda_{18}^i$ of $\Lambda_{18}^0$ discussed in section 10.5, by implementing a space-time renormalization of the lattice. To see this, we consider an initial condition in one of the subdomains, $\mathrm{s}_0 \in \Lambda_{18}^i$ for some given $i$, that itself consists of two adjacent patterns in $\Lambda_{18}^{i+1}$ separated by a dislocation $\Gamma_{18}^{(i+1)(i+1)}$. If this state is subjected to the operation of $\mathrm{T}_{\mathrm{decimate}(\Lambda^0)}$, the result is a state $\mathrm{s}_0' \in \Lambda_{18}^{i-1}$ consisting of two adjacent patterns in $\Lambda_{18}^i$ separated by a dislocation $\Gamma_{18}^{ii}$. As noted above, the decimated state $\mathrm{s}_0'$ evolves according to ECA 90. However, the actions of ECA 18 and ECA 90 are

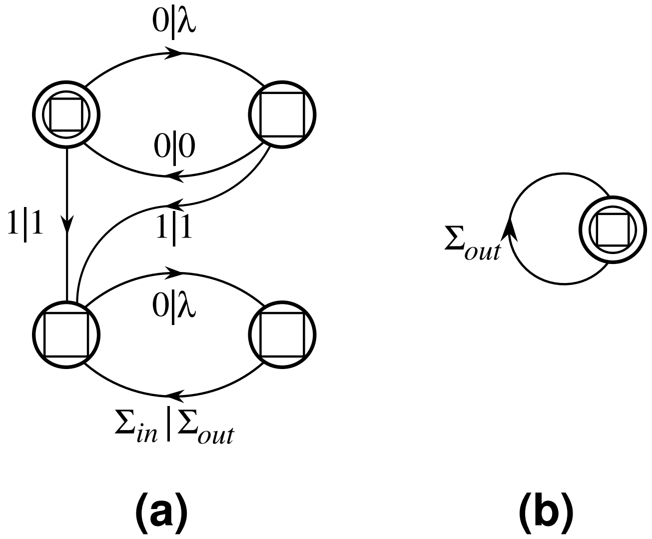


Fig. 12.4 (a) Transducer $\mathrm{T}_{\mathrm{decimate}}(\Lambda^0)$ for removing, in fact compressing or encoding, the patterns in $\Lambda^0$ into $\mathcal{A}^*$. The two transient states ensure that the machine synchronizes properly to strings beginning with any number of consecutive 0s. (b) The transducer has been minimized with respect to its output. The resulting automaton accepts $\mathcal{A}^*$.

identical on states in $\Lambda^0_{18}$, and therefore on states in $\Lambda^{i-1}_{18}$; so we can regard $\mathrm{s}'_0$ as evolving under ECA 18. This makes it possible to apply the decimation transducer $\mathrm{T}_{\mathrm{decimate}(\Lambda^0)}$ again, giving a state $\mathrm{s}''_0 \in \Lambda^{i-2}_{18}$ consisting of two adjacent patterns in $\Lambda^{i-1}_{18}$ separated by a dislocation $\Gamma^{(i-1)(i-1)}_{18}$. This renormalization procedure, repeated a total of $i+1$ times, yields a renormalized state $\mathrm{s}^{(i+1)}_0 \in \mathcal{A}^*$ consisting of two adjacent domains $\Lambda^0_{18}$ separated by a dislocation $\Gamma^{00}_{18}$—i.e., $\mathrm{s}^{(i+1)}_0 \in \Lambda^{0,0}_{18}$—evolving under ECA 90. The evolution of such a state was plotted in fig. 10.22. As the figure shows, the single dislocation at time $t = 0$ gives rise to a rapidly spreading cone of multiplying dislocations. In other words, the domain $\Lambda^0_{18}$ evolving under ECA 90 is *unstable* to perturbations within the larger set $\mathcal{A}^*$. Returning to the original sub-domain state $\mathrm{s}_0 \in \Lambda^i_{18}$, the consequence is that every sub-domain $\Lambda^i_{18}$ is unstable to perturbations within the larger set $\Lambda^{i-1}_{18}$.

## 12.6 The Attractor-Basin Portrait

We gather together the preceding results for an essentially graphical display of the global view of the attractor basin (AB) portrait of ECA 18. We present two views. The first is somewhat skeletal and is the picture provided by regular language space. The second is schematic and gives a cartoon of the state space of arbitrary but high dimension.

From the viewpoint of regular language space the AB portrait is relatively simple. We can identify the basic sets in a skeletal AB portrait in which the vertices of the graph are various languages. A skeletal picture of ECA 18's attractor-basin portrait as seen in regular language space is given in fig. 12.5. The various symbols indicate the formal languages identified in the computation theoretic analysis: attractors $\{\Lambda^0, \Lambda^{0,0}\}$, basins $B^0 = \mathcal{B}(\Lambda^0)$ and $B^{0,0} = \mathcal{B}(\Lambda^{0,0})$, and separatrices $\mathcal{S} = \{\mathcal{S}_{\text{even}}, \mathcal{S}_{\infty}, \mathcal{S}_{\text{odd}}\}$. The temporal evolution from one language to another goes down the figure. The context of this diagram is a lattice of arbitrary typical size $N$, either infinite or finite with periodic boundary conditions. If $N$ is odd, then only the portion to the right of the right vertical dashed line is observed. If $N$ is even, then only that to the left of the left dashed line is relevant. On an infinite lattice the entire diagram is present. The vertical dashed lines also denote the extent to which small perturbations can affect states in the attracting languages. A unit Hamming distance perturbation $\delta_r\Lambda$ from the attractor drives the state to its basin or, at worst, to a periodic orbit in the associated subset of the separatrix. In fact, topological constraints prohibit bit-flip perturbations within the nonzero support from driving the configuration to the other attractor. If the lattice is infinite and the initial patterns are restricted to a finite support of nonzero site values, then there are no separatrices, since all states eventually collapse onto one or the other attractor in finite time.[63] Unit Hamming distance perturbations outside the region of nonzero sites in a state then can introduce single dislocations and so move the state from $B^0$ to $B^{0,0}$, and visa versa. The subseparatrices $\mathcal{S} = \{\mathcal{S}_{\text{even}}, \mathcal{S}_{\infty}, \mathcal{S}_{\text{odd}}\}$ are disjoint. $\mathcal{S}_{\text{even}}$ and $\mathcal{S}_{\text{odd}}$ consist of temporally periodic patterns with an even and odd number of dislocations greater than one asymptotically in time, respectively. $\mathcal{S}_{\infty}$ contains all aperiodic patterns with more than one dislocation, and all patterns with an infinite number of dislocations, in the limit $t \to \infty$. All states in $\mathcal{S}_{\infty}$ have infinite nonzero support. As noted in section 12.4, we omit from the diagram (i) behavior on the sparse set of atypical lattices for which $0^*$ is an important attracting invariant set and (ii) on the remaining lattices, the zero-sized set $\mathcal{B}(0^*)$. The nonattracted sets of zero size are collected in the separatrices.

Much more can be said about the configuration space itself. Generally, local particle annihilation dynamics induces a hierarchical structure of subbasins and portals.[17] The subbasins are subspaces in which the number of dislocations is constant. Thus they are level sets of the machine metric: $b_d = \left\{ \mathrm{s} : \|\mathrm{s}\|_{\mathrm{M}(\Lambda^0)} = d \right\}$. In this notation, the subbasin vicinities defined in section 12.1 are given by $V_b(\Lambda^0) = b_0 \cup b_2$ and $V_b(\Lambda^{0,0}) = b_1 \cup b_3 \cup 0^*$. The subbasins are connected by portals which are defined solely in terms of the particle annihilation geometry. Since the number of dislocations cannot increase, there is a flow directed from higher to lower dimensional subspaces. Here by "dimension" we refer to the number of "active" degrees of freedom which we take to be the number of dislocations. In the transition from a $d$-subbasin $b_d$, caused by two dislocations annihilating, the number of dislocations decreases by two. This moves the state from a $d$-subbasin to a $(d-2)$-subbasin. It is also possible for more than one pair of dislocations to annihilate in one time step, in which case the state falls into a $(d-2m)$-subbasin, where $m$ is the number of annihilating pairs. The subbasin-portal structure is shown schematically in fig. 12.6.

The intercalation operator $f_{\mathrm{T}_{\text{intercalate}}(\Lambda^0)}$ maps the configuration space of an $N$-site lattice containing $d$ dislocations to the domain subspace of a $(N+d)$ lattice on which

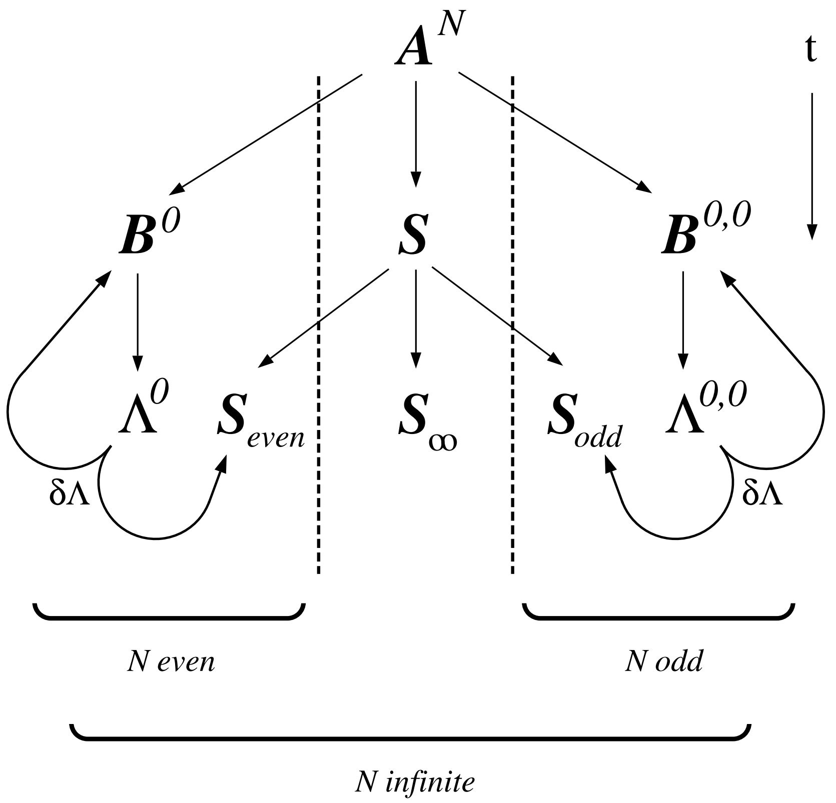


Fig. 12.5 A skeletal picture of ECA 18's attractor-basin portrait as seen in language space. The various symbols indicate the formal languages identified in the computation theoretic analysis. The temporal evolution from one language to another goes down the page. The thin lines with arrows indicate the effect of perturbations $\delta\Lambda$ away from the attractors.

the rule is linear.[63] This gives an additional hierarchical constraint to the state space.

It is important to point out that the state space structures implied by the portal concept and the intercalation operator are not the same. Portals, on the one hand, are local in the state space and their geometric structure is entirely determined by the local "real" space constraints on particle annihilation. The intercalation operator, on the other hand, is global in both the state and "real" spaces. The result is that the portals still organize the state space of multiple distinct-domain dynamics, a situation in which the global intercalation operator does not exist. Indeed, the underlying views behind each are complementary. Understanding their relationship is certain to lead to an even more detailed picture of the state space geometry of domain-wall dominated CA than that presented here.

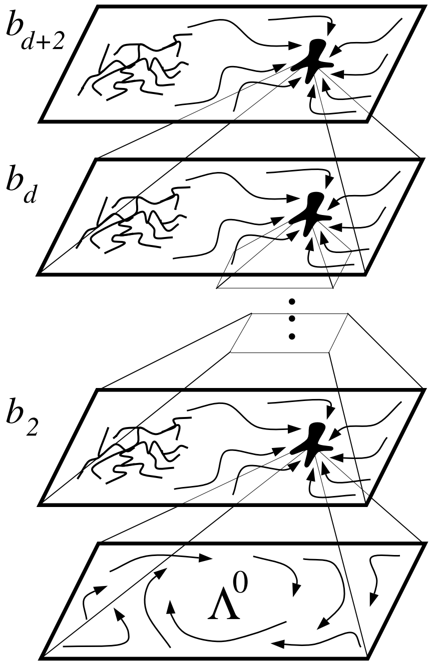


Fig. 12.6 The state-space view of the attractor-basin portrait of ECA 18 for an even length lattice or, equivalently, the left-most portion of fig. 12.5. The diagram illustrates the subbasin-portal structure of the state space.[17] One subbasin corresponds to each horizontal plane. Within each subbasin $b_d$, the number of dislocations $d$ is constant. The portal is indicated by the solid dark blob. When pairs of particles annihilate the state passes through the portal. Its shape is determined by the geometric constraints of annihilation. That portion of the separatrix consisting of configurations with the subbasin's number of dislocations is shown as a filamentary structure to denote its vanishing relative size. The general flow of time is down the figure. Asymptotically in time and lattice size, the overwhelming fraction of initial patterns in $V^0$ end up on the attractor $\Lambda^0$, all of the dislocations having annihilated.

# 13 Vicinity Convergence in ECA 18

This chapter continues the investigation of ECA 18's regular attractors by examining their stability under small perturbations in each attractor's vicinity. First we consider the temporal evolution of the vicinity, tracing its decay back onto the attractor.* Then we examine the lattice-size dependence of the vicinity's asymptotic statistics.

## 13.1 Temporal Vicinity Convergence

As we have seen, there are several alternatives for the vicinity, such as (i) the subbasin vicinities $V_b(\Lambda)$ with $\Lambda = \Lambda^0$ on even lattices or $\Lambda = \Lambda^{0,0}$ on odd lattices, or (ii) the Hamming vicinity $V_H(\Lambda)$. The latter, in which perturbations are spatially localized, is the more physically realistic of the two if one thinks of the perturbations as being due to thermal fluctuations. Typical states in the subbasin vicinity require perturbations correlated over long distances. For this reason, we will focus primarily on the Hamming vicinity in the following. The perturbation we consider, arguably the "smallest" one possible, is a single bit-flip somewhere in the state. If the site flipped is not a wild-card site, this perturbation pushes the state off the attractor by generating a pair of dislocations, which then move about on the lattice and ultimately may or may not collide and annihilate. If and when the dislocations annihilate, the state falls back into the attractor.

Under the action of ECA 18 not all of the patterns in the Hamming vicinity fall back into the attractor, even asymptotically. Thus, on lattices with even size $N$, the vicinity $V^0 \equiv V_H\left(\Lambda^0\right)$ breaks up into two disjoint subsets, determined by the two possible asymptotic $(t \to \infty)$ behaviors: (i) the set $E^0$ of states that eventually evolve back into the attractor, and (ii) the set $P^0$ of states that evolve onto temporally periodic orbits not in $\Lambda^0$. By definition, $E^0 = B^0 \cap V^0$ and $P^0 = S_{even} \cap V^0$ where $B^0$ and $S_{even}$ are the basin and separatrix associated with $\Lambda^0$, as described in section 12.6. In fig. 12.5, these two possible asymptotic behaviors were indicated by the two curved lines leading away from $\Lambda^0$. For $N$ odd, the situation is analogous, with the vicinity $V^{0,0}$ breaking up into $E^{0,0}$ and $P^{0,0}$. In the following we will consider $\{V, \Lambda, E, P\}$ to be $\left\{V^0, \Lambda^0, E^0, P^0\right\}$ for $N$ even, and to be $\left\{V^{0,0}, \Lambda^{0,0}, E^{0,0}, P^{0,0}\right\}$ for $N$ odd.

The states in the Hamming vicinity are generated by a two step process. First, a state is produced using the appropriate attractor machine $M(\Lambda)$. Second, a site is selected at random and its value is set randomly to $0$ or $1$. With probability $\frac{1}{2}$ this changes the state; the result may or may not be in the attractor. And with probability $\frac{1}{4}$ a pair of dislocations is created, knocking the pattern off the attractor into the vicinity. The resulting interdislocation distance $d > 0$ is distributed exponentially as

$$Pr(d = x) = \begin{cases} 2^{-\frac{x+1}{2}} & x = 1, 3, 5, \ldots \\ 0 & \text{otherwise} \end{cases} \tag{13.1}$$

*This work originally appeared in ref. [24].

An ensemble with $M$ members generated in this way will have at $t = 0$ approximately $M/4$ patterns off the attractor.

A vicinity ensemble's decay can be monitored by the fraction $f_\Lambda(t)$ of ensemble states on the attractor as a function of time. For a fixed lattice size at a given time, we define the complementary fraction $f_P(t)$ of nonattracted patterns in the vicinity ensemble as

$$f_P(t) = \frac{\left\|\mathbf{\Phi}^t(V) - \Lambda\right\|}{\|V\|}. \tag{13.2}$$

The set-theoretic difference $\mathbf{\Phi}^t(V) - \Lambda$ denotes the ensemble of states in $\mathbf{\Phi}^t(V)$ not yet on the attractor. Clearly, $f_P(t)$ is monotonically nonincreasing with $t$, and $f_\Lambda(t) + f_P(t) = 1$. The asymptotic nonattracted fraction is given by

$$f_P = \lim_{t \to \infty} f_P(t) \tag{13.3}$$

We define the convergence time $T_c$ as the first time-step at which $f_P(t)$ reaches its asymptotic value. Note that on any given finite lattice $f_P$ is equal to $\|P\|/\|V\|$, the fraction of vicinity states evolving to periodic orbits not on the attractor.

The decay profile $f_P(t)$ gives an indirect indication of the orbit structure of the high-dimensional state space. On a finite lattice with periodic boundary conditions, all states eventually fall onto temporally periodic orbits. In particular, starting from any given initial state $\mathrm{s}_0$ in the vicinity $V$, the trajectory $\{\mathrm{s}_1, \mathrm{s}_2, \mathrm{s}_3, ...\}$ will at some point fall onto a periodic orbit either in the attractor $\Lambda$ or in the nonattracted set $P$. If this orbit is in $\Lambda$, then there is a time $\tau$ at which it first fell into $\Lambda$. We therefore define a transient starting in $V$ in the following fashion.

**Definition.** A **transient starting in *V*** is a sequence of states $\{\mathrm{s}_0, \mathrm{s}_1, ..., \mathrm{s}_{\tau-1}\}$ such that (i) the initial state lies in the vicinity: $\mathrm{s}_0 \in V$; (ii) the last state is not in the attractor: $\mathrm{s}_{\tau-1} \notin \Lambda$; and (iii) the iterate of the last state is in the attractor: $\mathrm{s}_\tau = \Phi(\mathrm{s}_{\tau-1}) \in \Lambda$.

This is a somewhat different notion of transient that is used in the "transients and cycles" analysis described in section 2.3; in particular, $\mathrm{s}_\tau$ need not be on a periodic cycle. Note also that this definition excludes states in $P$. All states on transients starting in the Hamming vicinity have two dislocations if $N$ is even, or three dislocations if $N$ is odd. The transient length $\tau$ is equal to the number of states in that part of the trajectory that lies outside $\Lambda$. The fraction of states in the ensemble with transient length $\tau$ is given by the instantaneous decay rate

$$\Delta f_P(\tau) \equiv f_P(\tau) - f_P(\tau - 1). \tag{13.4}$$

In this way, the decay curve $f_P(t)$ is the integral of the transient-length probability density. Furthermore, since $f_P(t)$ can change only while there are states on transients, $T_c$ is equal to the length of the longest transient. What $f_P(t)$ fails to capture is the detailed architecture of the state space, i.e., the connectivity of the trajectories.

## 13.2 Random Cliff Walkers

In ECA 18, the final decay of an arbitrary initial pattern to the attractor usually reduces to the annihilation of only two dislocations. On an even lattice two dislocations collide leaving a pattern on the attractor $\Lambda^0$ with none; on an odd lattice two of three collide leaving a pattern on $\Lambda^{0,0}$ with one dislocation. The stochastic analog of the net process is that the dislocations diffuse according to a random walk and two of them eventually annihilate when their paths cross. The question in this view becomes whether ECA 18 with patterns restricted to the vicinity behaves effectively like a stochastic process.

A crude approximation of dislocation evolution, valid in the limit of vanishing dislocation density, was given in ref. [47]. That probabilistic model is inadequate for Hamming vicinity decay since, as just noted in eq. 13.1, the dislocation density is weighted toward small separations. As an alternative, we now describe the *random cliff walker* (RCW), a simple stochastic process that captures the basic phenomenon. The RCW model, and modifications described below, are variants of a random walk with absorbing barriers.[38,94]

In an ideal random walk a particle moves left or right with equal probability. The distance $d(t)$ between two such particles either stays the same or changes with equal probability. If the distance does change, it increases or decreases by two units, again with equal probability. In the RCW process two particles annihilate whenever the distance passes through zero. $d(t)$ itself can be considered as a quasiparticle obeying a random walk on the half-line $d > 0$. In effect, there is a *cliff* at the origin: when dislocations annihilate, $d$ passes through zero and the random walker falls off the cliff. This is modeled by stopping the evolution of $d(t)$ at that point, effectively removing one pattern from the ensemble. The evolution rule for the RCW stochastic process is given by

$$d(t) = d(t-1) + \delta \qquad (13.5)$$

where $\delta$ is a random variable with the probability distribution given in table 13.1. The lattice constant has been changed to $1/2$ so that the possible displacements are $\delta \in \{-1, 0, +1\}$. For convenience, we allow $d(t)$ to take on negative values, but require that quasiparticles with $d(t) \leq 0$ be frozen in place.

| Random Cliff Walker | $d(t-1) \leq 0$ | $d(t-1) > 0$ |
|---|---|---|
| $Pr(\delta = +1)$ | 0 | $1/4$ |
| $Pr(\delta = 0)$ | 1 | $1/2$ |
| $Pr(\delta = -1)$ | 0 | $1/4$ |

Table 13.1. Stochastic evolution of the random cliff walker. The distance between particles evolves according to $d(t) = d(t-1) + \delta$.

Hamming-vicinity decay is simulated by generating an ensemble of $M$ RCW quasiparticles with an exponential distribution like that for the Hamming vicinity (eq. 13.1), namely

$$Pr(d(0) = x) = \begin{cases} 2^{-x-1} & x \geq 0 \\ 0 & x < 0 \end{cases} \tag{13.6}$$

The fraction $f_{RCW}(t)$ of surviving particles, i.e. those particles $i$ with $d_i(t) > 0$, is estimated using the statistic

$$f_{RCW}(t) = M^{-1} \sum_{i=0}^{M-1} \Theta_i(t), \tag{13.7}$$

where $\Theta_i(t)$ is the step function:

$$\Theta_i(t) = \begin{cases} 1 & d_i(t) > 0 \\ 0 & d_i(t) \leq 0 \end{cases} \tag{13.8}$$

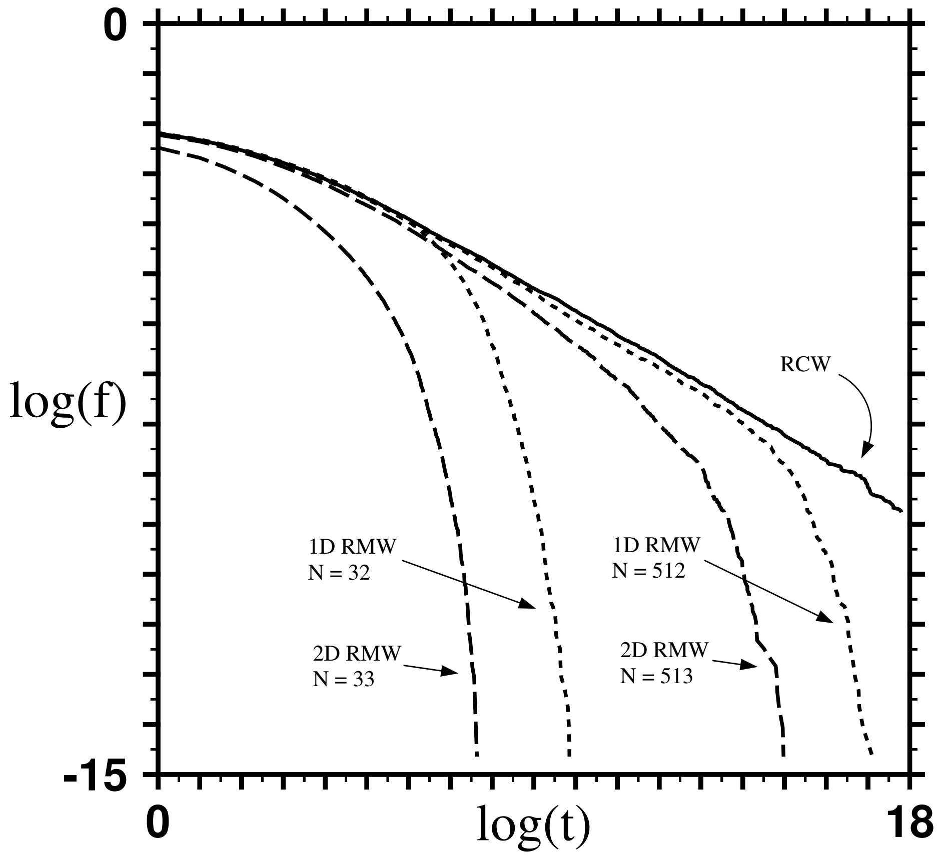


Fig. 13.1 Decay profiles for annihilating random walks. The random cliff walker decay profile $f_{RCW}(t)$ is the solid line. 1D and 2D random mesa walker profiles $f_{RMW}(t)$ are shown for lattices $N \in \{32, 512\}$ and $N \in \{33, 513\}$, respectively. In this and succeeding plots, logarithms are base 2. The simulations were performed with ensembles of size $M = 10,000$ for the RCW profile and $M = 12,800$ for each of the RMW profiles.